

Article

Terahertz Resonators based on Y-Ba-Cu-O High-Tc Superconductor

Salvatore Macis ^{1,2,†*}, Maria Chiara Paolozzi ^{3,†}, Annalisa D'Arco ^{1,2}, Luca Tomarchio ^{1,4}, Alessandra Di Gaspare ⁵ and Stefano Lupi ^{1,4}

¹ Department of Physics, Sapienza University, Piazzale Aldo Moro 5, 00185, Rome, Italy

² INFN - Laboratori Nazionali di Frascati, via Enrico Fermi 54, 00044, Frascati (Rome), Italy

³ Department of Science, Roma Tre University, Viale Guglielmo Marconi, 446, 00146, Rome, Italy

⁴ INFN section of Rome, PLe Aldo Moro, 2, 00185 Rome, Italy

⁵ NEST, CNR-Istituto Nanoscienze—Scuola Normale Superiore, 56127 Pisa, Italy

* Correspondence: salvatore.macis@uniroma1.it

† These authors contributed equally to this work.

Abstract: Superconducting split ring resonator arrays allow to overcome two main limitations affecting metallic metamaterial resonating in the Terahertz (THz) range: Ohmic losses and tunability of their optical response. In this work we design and experimentally realize direct and complementary square arrays of superconducting $\text{YBa}_2\text{Cu}_3\text{O}_7$ (YBCO) split ring resonators working in the THz spectral range. The main purpose of this paper is to show how the metamaterial resonances can be tuned by temperature (T) when crossing the superconducting transition temperature T_c of YBCO. The tuning property can be quantified by describing the THz transmittance of the patterned YBCO films vs. T through a model of coupled resonators. This model allows us to estimate the THz resonances of split-ring arrays and their interaction, showing how the the kinetic inductance L_k in the superconducting state is the main parameter affecting the metamaterial properties.

Keywords: split ring resonator; superconductor; modulation; THz

1. Introduction

Metamaterials (MMs) are artificial engineered systems exhibiting a geometrically scalable electric and/or magnetic resonant response in a broad spectral range from microwaves to visible [1–9]. Indeed, thanks to specific patterning, the optical response of these systems can be engineered with respect to the original material, paving the way to innovative opto-electronic applications.

The most widely spread MMs are constituted of periodically patterned thin metallic films deposited on a dielectric substrate, enabling to trigger unusual electromagnetic properties, ranging from superlenses [10], sensors [11,12], light induced transparency [13], chiral devices [14], filters [15], and modulators [16]. However, two main issues limit the practical applications of metallic metamaterial devices: Ohmic losses and tunability. For operational frequencies increasing toward the terahertz (THz), infrared and visible range, Ohmic losses are strongly enhanced, reducing the quality factor of resonances and therefore their tunability. To overcome these drawbacks, the use of superconducting materials has been proposed [17][18]. As a matter of fact, the low-loss properties of superconductors at finite frequency and their sensitivity to external stimuli, such as temperature, magnetic field and light-pulses, can be exploited to provide a robust tunability of the device response. More specifically, High Temperature Superconductor Cuprates (HTSCs) are the suitable candidate for facing this challenge since they provide a much broader frequency range of tunability compared to conventional Bardeen–Cooper–Schrieffer (BCS) superconductors, extending beyond 10 THz [19]. In this work, we report on the fabrication and optical response in the THz spectral range of square arrays of direct and complementary split ring resonators (SRRs) composed of High-Tc cuprate YBCO (see Figure 1a and 1b respectively). The temperature modulation of their THz resonances has been described in terms of a circuit representation (commonly used in the microwave spectral range and extended to

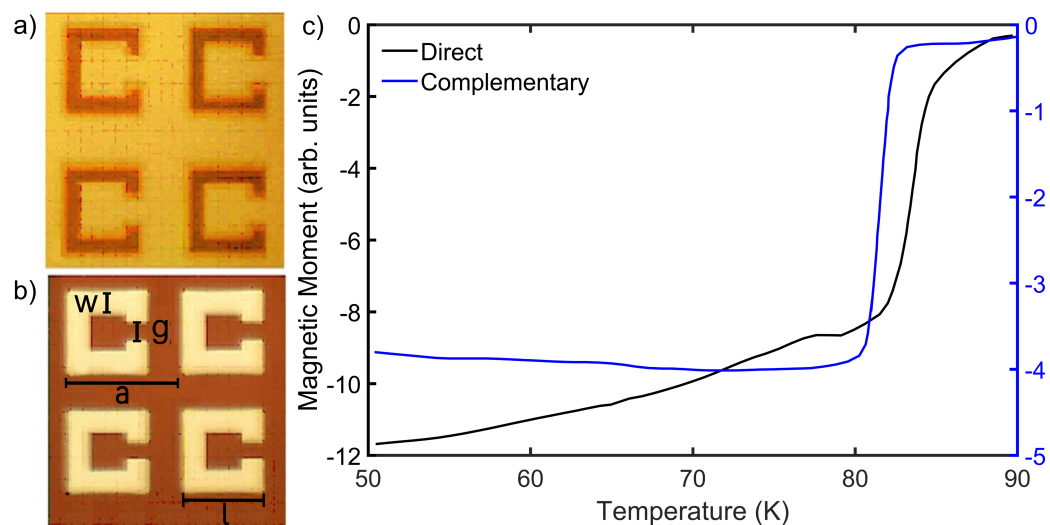


Figure 1. SEM pictures of the direct (a) and complementary (b) SRR devices. Dark areas mark YBCO film while light areas Al_2O_3 substrate. The geometrical details are $l = 20 \mu m$, $g = 5 \mu m$, $w = 5 \mu m$ and $a = 30 \mu m$. (c) Magnetic moment measurements for the direct and the complementary device, respectively.

THz), according to which SRRs act as an RLC circuit, taking into account both the THz response of the single split-ring resonator and their collective interactions. We experimentally determine the surface impedance Z_s and kinetic inductance L_k of SRRs from the temperature dependence of the THz resonances, induced by the increasing inductive response when the temperature is lowered below T_c . The experimental determination of the kinetic inductance is of fundamental importance, being it responsible for the tuning of the metamaterial optical response.

2. Materials and Methods

2.1. YBCO Film Synthesis and Patterning

Direct and complementary split ring resonator square arrays (see Figure 1a and b), were fabricated through electron beam lithography (EBL) on commercial 200 nm thick optimally doped $YBa_2Cu_3O_7$ films grown on a 500 μm thick sapphire (Al_2O_3) substrate. YBCO films, provided by THEVA (Germany), were grown by reactive thermal coevaporation and exhibit an average surface roughness of 6-10 nm. The desired metamaterial pattern was transferred by electron beam lithography to a resist coating and a wet etching in 0.075 % nitric acid, allowing the removal of the non-covered YBCO. Metamaterial parameters were chosen to have both the LC and dipolar resonance frequencies in the 0.5 to 4 THz range, below the YBCO superconducting gap. Figure 1a and 1b show Scanning-Electron-Microscopy (SEM) pictures of the direct and complementary MMs together with their geometrical details. The single SRR has a side length $l = 20 \mu m$, width $w = 5 \mu m$ and gap $g = 5 \mu m$, while the SRR lattice parameter is $a = 30 \mu m$. Dark areas refer to YBCO film whereas light areas to the Al_2O_3 substrate. As it can be inferred, the complementary structure shares the same geometry of the direct one, with inverted YBCO and Al_2O_3 . To measure the superconductive properties of the patterned film, magnetic moment measurements were performed on both direct and complementary samples, as a function of temperature. Figure 1c shows that the direct SRR array has a critical temperature $T_c = 83$ K in agreement with the nominal value from THEVA, while the complementary one has a slightly lower T_c of ~ 81 K. The slight shift in T and the reduced jump in the magnetic moments at T_c are probably related to the differences in YBCO content between the direct and complementary patterned films.

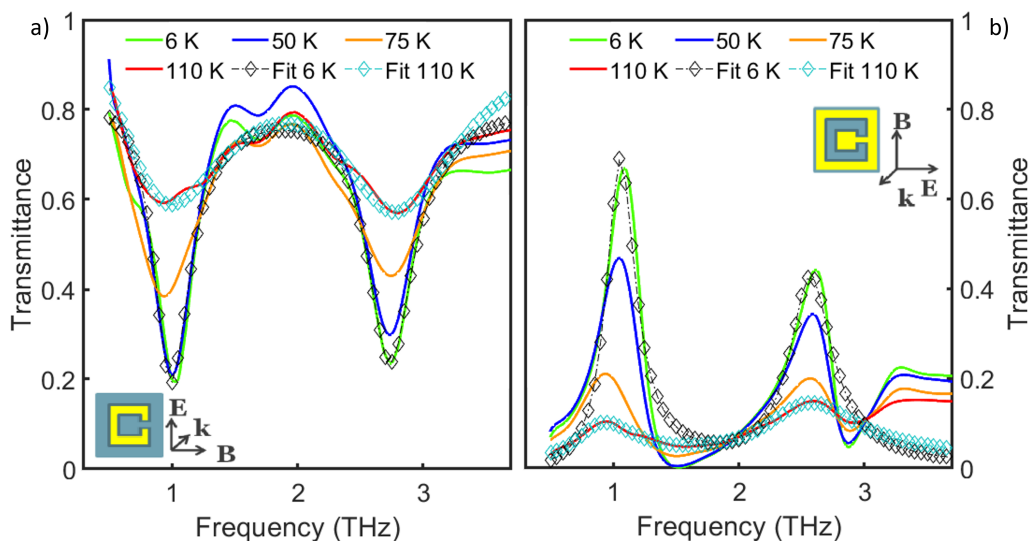


Figure 2. Experimental transmittance spectra for direct (a) and complementary (b) SRR arrays at different temperatures. In both cases, the fitting curves (empty symbols) at 6 K and 110 K are reported, too. The insets show a sketch of the corresponding SRR geometry with the electric field polarization perpendicular with respect to the SRR gap (a) and parallel with respect to the CSRR gap (b). Yellow areas indicate YBCO, light-blue areas Al_2O_3 substrate.

2.2. Optical Measurements

Fourier transform infrared spectroscopy (FTIR) transmission measurements in the THz range were carried out with a Bruker Vertex 70v spectrometer, scanning from 0.5 to 4 THz. An Infrared Labs Germanium Bolometer detector was used in this spectral range. A continuous-flow liquid helium cryostat was employed to perform transmittance measurements at temperatures ranging from 6 K up to 110 K with an uncertainty of 0.5 K. The transmittance of the arrays was measured at normal incidence and normalized with respect to the one of the bare sapphire substrate. The SRR array optical response is sensitive to the electric field polarization [20][21]. Therefore, to maximize the metamaterial response, measurements were performed with the radiation electric field perpendicular to the gap for the direct device, and parallel to the gap for the complementary one. On this regard, a polyethylene-based metallic wire polarizer with an efficiency of 99 % has been used. The transmittance spectra at different temperatures were analysed with the MATLAB® software in order to assess the temperature dependence of the parameters associated to the metamaterial resonances (see Figure 2).

3. Results and Discussion

As previously mentioned normal-incidence transmittance measurements were performed on both direct and complementary SRRs in the range from 0.5 to 4 THz at different temperatures, ranging from 6 K to 110 K and crossing T_c . For each temperature, the transmittance was normalized with respect to the one of the bare sapphire substrate, to isolate the SRR contribution. Figure 2 shows the normalized transmittance for both direct and complementary devices at four different temperatures. The fitting curves (empty symbols) at 6 K and 110 K are shown as well. More specifically, Figure 2a reports the transmittance spectra for the direct device, with the electric field polarized perpendicular to the SRR gap, and Figure 2b for the complementary one, with the electric field polarization rotated by 90, as shown in the insets and in agreement with the Babinet principle [22][23]. When the electric field is polarized perpendicular to the SRR gap (for the direct case), two main resonances appear. The one at lower frequency (located at about 1 THz), is called LC resonance [24] since the electric field couples with the geometric capacitance and inductance of the SRR, generating a closed resonant circulating current inside the metallic ring. This

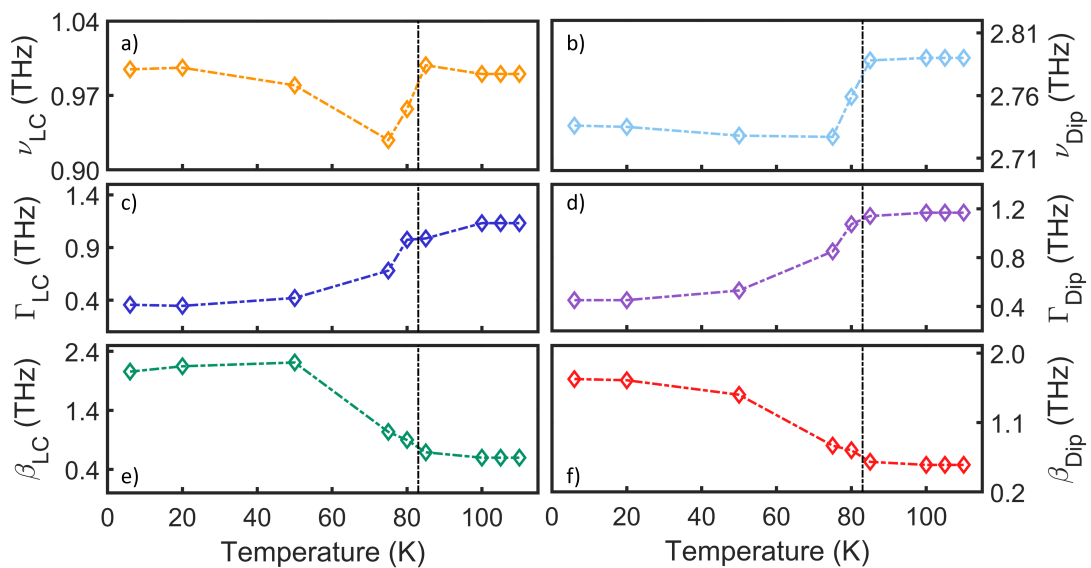


Figure 3. Fitting results (empty symbols) for the direct SRR device vs. T as obtained by using Equation 1 applied to data in Figure 1a. The dashed color lines are a guide for the eyes. (a),(c) and (e) show the resonance frequency ν_{LC} , the linewidth Γ_{LC} and the coupling coefficient β_{LC} of the LC resonance; (b),(d) and (f) show the the same quantities for the dipolar resonance. The black vertical point-dashed lines underline YBCO critical temperature $T_c = 83$ K.

resonance is also defined as "magnetic" because the time-varying current creates a magnetic dipole moment perpendicular to the ring plane. The second resonance, instead, appears at higher frequency (around 2.7 THz) and is called dipolar because it is characterized by the excitation of an electric dipole along the SRR arm opposite to the gap. These features appear as dips in the direct device and as peaks in the complementary one, and get broader and weaker for increasing temperature.

The transmittance $T_{dir}(\nu, T)$ of the direct array (complementary, $T_{comp}(\nu, T) = 1 - T_{dir}(\nu, T)$) can be expressed through the following equation [25]:

$$T_{dir}(\nu, T) = T_0 \frac{1 + (1 + \frac{\beta_{LC}}{2})^2 Q_{L,LC}^2 (\frac{\nu}{\nu_{LC}} - \frac{\nu_{LC}}{\nu})^2}{1 + Q_{L,LC}^2 (\frac{\nu}{\nu_{LC}} - \frac{\nu_{LC}}{\nu})^2} \frac{1 + (1 + \frac{\beta_{Dip}}{2})^2 Q_{L,Dip}^2 (\frac{\nu}{\nu_{Dip}} - \frac{\nu_{Dip}}{\nu})^2}{1 + Q_{L,Dip}^2 (\frac{\nu}{\nu_{Dip}} - \frac{\nu_{Dip}}{\nu})^2} \quad (1)$$

where T_0 is the transmittance level far from the resonances, ν_{res} ($res = LC, Dip$) is the resonance frequency, $Q_{L,res} = \frac{\nu_{res}}{\Gamma_{res}}$ is the loaded quality factor, Γ_{res} being the resonance width, and β_{res} is the coupling coefficient among different resonators. This equation, usually used in the microwaves region [25], takes into account both the resonating behavior of the single split-ring and their mutual interaction through the β coefficients.

Equation 1 well fits experimental data as shown for two representative temperatures (6 and 110 K) in Figure 2a and b by open symbols. From the fitting we extracted the temperature dependence of ν_{res} , Γ_{res} , and β_{res} which are represented in Figure 3 and 4 for the direct and complementary array, respectively. All the parameters exhibit a variation in temperature. More in detail, for the direct SRR array, both the LC and dipolar resonance frequencies display a non-monotonic behavior with temperature with a dip slightly below T_c (black vertical point-dashed line), corresponding to a redshift of 8 % and 2 % for the LC and dipolar resonance frequencies, respectively. The linewidth for both resonances exhibits a step-like behaviour: from 110 K until 6 K the linewidth of both LC and dipolar resonances decreases by a factor $\simeq 3$, improving resonance selectivity. Finally, the coupling coefficient among different resonators (β) shows a robust increasing behavior while going from the normal to the superconducting phase. In particular, for both resonances, β is nearly zero in the normal state indicating a negligible interaction among split-ring resonators. This

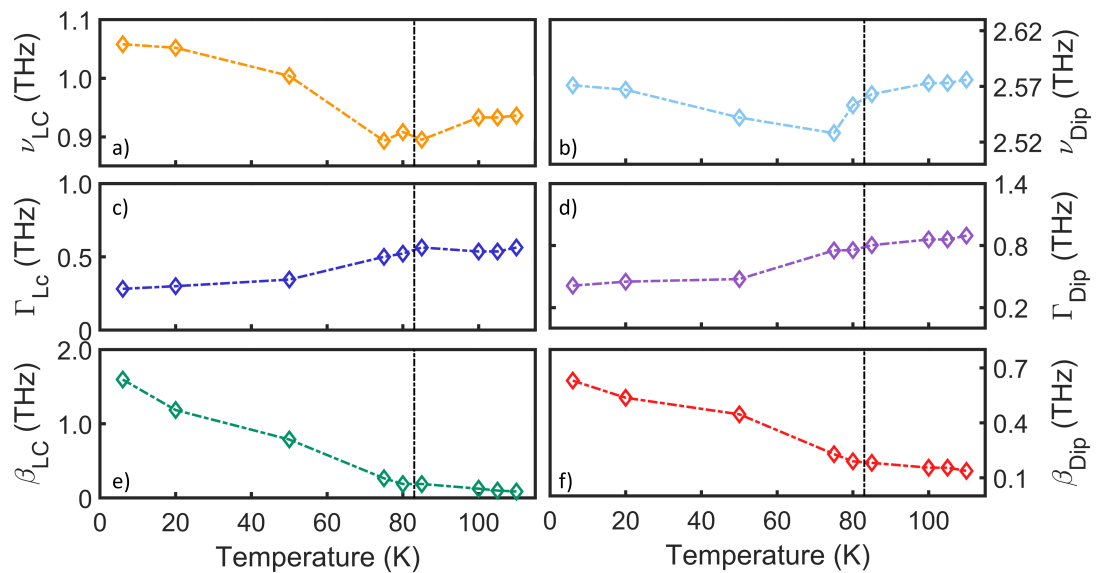


Figure 4. Fitting results (empty symbols) for the complementary SRR device vs. T as obtained applying Equation 1 to data in Figure 1b. The dashed color lines are a guide for the eyes. (a), (c) and (e) show the resonance frequency ν_{LC} , the linewidth Γ_{LC} and the coupling coefficient β_{LC} of the LC resonance; (b), (d) and (f) show the same quantities for the dipolar resonance. The black vertical point-dashed lines underline YBCO critical temperature $T_c = 81$ K.

interaction strongly increases in the superconducting state, and the positive sign of both β indicates that both the electric and magnetic fields are involved in the resonator coupling, as explained in [26].

In the complementary SRR device a similar trend is observed for all the parameters. A modulation of 18 % and of 2 % for the LC and dipolar resonance frequencies is observed, respectively. Similarly to the case of the direct device, the linewidth for both resonances decreases by a factor $\simeq 2$. Finally, the coupling coefficient β changes by a factor 18 for the LC resonance, and by a factor 5 for the dipolar one. Table A1 and Table A2 report the loaded quality factors of both LC and dipolar resonances for direct and complementary devices as a function of temperature. For both devices, the dipolar resonance has a higher quality factor than the LC one, and for both the resonances the quality factors increase by reducing temperature due to the reduction of Ohmic losses. In light of the aforementioned results, kinetic inductance of the SRR arrays can be calculated to understand how the onset of the superconducting state affects the metamaterial optical response. This parameter can be obtained from the relation $L_k \simeq (p/w)(X_s/2\pi\nu)$, where p is the SRR perimeter, w its width, X_s the surface reactance, i.e. the imaginary part of the surface impedance Z_s , and ν the frequency [27]. Being a property of the YBCO film, the surface impedance was extracted from the complex optical conductivity as measured in an unpatterned YBCO film at the LC resonance frequency [28–30]. The real part of the surface impedance determines the power absorption in a metal, caused by non-superconducting carriers, while the imaginary part accounts for the phase difference between incident electric field and the induced current density in the material and is largely determined by superconducting Cooper pairs [31]. In the superconducting state, X_s dominates over R_s , whereas in the normal state the opposite holds. Figure 5 reports the real and imaginary parts of the surface impedance (a) as a function of temperature, and the kinetic inductance as a function of temperature for both direct and complementary SRRs calculated at the LC resonance frequency (b). As it can be noticed, the kinetic inductance has a maximum near T_c , directly affecting the strong variation of both LC and dipolar resonance frequencies around this temperature. Indeed, in a first approximation, $\nu_{res} = 1/2\pi\sqrt{(L_g + L_k)C}$, where C , L_g and L_k are the capacitance, the geometric and the kinetic inductance of the resonators. Therefore the maximum in

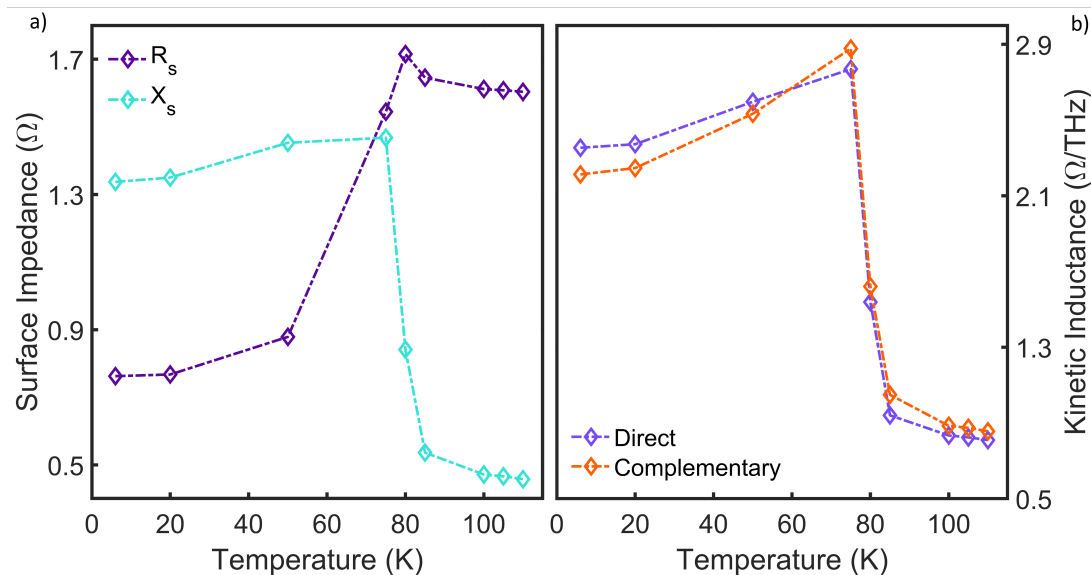


Figure 5. (a) Surface resistance (R_s) and reactance (X_s) associated to the unpatterned YBCO film as a function of temperature. The complex quantity was calculated by using experimental complex conductivity of the unpatterned YBCO film at the LC resonance frequency. (b) Kinetic inductance calculated at the LC resonance frequency for both direct and complementary devices.

Figure 5b explains the minimum of the LC and dipolar resonance frequencies around T_c . This trend was already observed in other superconducting metamaterials, as described in Reference [32].

4. Conclusions

In this work we demonstrated that High- T_c $\text{YBa}_2\text{Cu}_3\text{O}_7$ superconductor can be employed to tune the split-ring resonator optical response in the Terahertz spectral range by crossing the critical temperature of the superconductor. Interpreting SRRs as RLC circuits, we demonstrated that for $T < T_c$ the inductive response (X_s) of the circuit dominates over the resistive one (R_s), inducing a modulation of the optical response of both direct and complementary devices. More specifically, the reduction of ohmic losses due to the superconducting transition makes LC and dipolar resonances stronger, with smaller linewidths and larger coupling coefficients. Moreover, the strong increase of the kinetic energy and therefore of the kinetic inductance L_k in the superconducting state introduces a huge modulation of the resonances. Different superconducting metamaterial geometries including fractal [33] and magnetic field enhancing shapes [34] will be investigated in the future to further study their use for opto-electronic applications.

Author Contributions: All authors contributed extensively to the work presented in this paper. S.M. and S.L. designed the experiment. S.L., S.M. and M. C. P. supervised the work. A. Di G. prepared the films and fabricated the SRR patterning. M.C.P. and S.M. developed the theoretical model. S. M., M. C. P., A.D. and L.T. performed the optical measurements and SEM images. M.C.P. analyzed the data. S.M., M.C.P. and S.L. prepared the original draft. All authors reviewed the manuscript.

Funding: This work has received the financial support by INFN institute in the framework of the project of major relevance TERA and PbT.

Data Availability Statement: The datasets generated and analysed during the current study are not publicly available due to Department policy but are available from the corresponding author on reasonable request.

Conflicts of Interest: The authors declare no conflict of interest.

Appendix A

Appendix A.1 LC and dipolar resonances quality factors

In the following the loaded quality factors associated to both LC and dipolar resonances of direct and complementary devices as a function of temperature are reported.

Table A1. Loaded quality factors associated to both LC and dipolar resonances for direct device at different temperatures.

Temperature (K)	$Q_{L,LC}$	$Q_{L,Dip}$
6 K	2.79	6.05
20 K	2.87	6.05
50 K	2.32	5.14
75 K	1.36	3.20
80 K	0.98	2.57
85 K	1.01	2.45
100 K	0.88	2.39
105 K	0.88	2.39
110 K	0.88	2.39

Table A2. Loaded quality factors associated to both LC and dipolar resonances for complementary device at different temperatures.

Temperature (K)	$Q_{L,LC}$	$Q_{L,Dip}$
6 K	3.75	6.23
20 K	3.51	5.69
50 K	2.91	5.34
75 K	1.79	3.36
80 K	1.74	3.38
85 K	1.59	3.19
100 K	1.74	3.00
105 K	1.74	3.00
110 K	1.67	2.89

References

1. Bilotti, F.; Sevgi, L. Metamaterials: Definitions, Properties, Applications, and FDTD-Based Modeling and Simulation. *Int. J. RF Microw. Comput.-Aided Eng.* **2012**, *22*, 422–438.
2. Liu, Y.; Zhang, X. Metamaterials: a new frontier of science and technology. *Chem. Soc. Ref.* **2011**, *40*, 2494–2507.
3. Capolino, F. *Theory and Phenomena of Metamaterials*, 3rd ed.; CRC Press: Publisher Location, Country, 2009.
4. Johnson, N.P.; Khokhar, A.Z.; Chong, H.M.; De La Rue, R.M.; Antosiewicz, T.J.; Mcmeekin, S. A Review of Size and geometrical Factors influencing resonant Frequencies in Metamaterials. *Opto-Electron. Rev.* **2006**, *14*, 187–191.
5. Di Pietro, P.; Adhlakha, N.; Piccirilli, F.; Di Gaspare, A.; Moon, J.; Oh, S.; Di Mitri, S.; Spampinati, S.; Perucchi, A.; Lupi, S. Terahertz Tuning of Dirac Plasmons in Bi_2Se_3 Topological Insulator. *Phys. Rev. Lett.* **2020**, *124*, 226403.
6. D'Apuzzo, F.; Piacenti, A. R.; Giorgianni, F.; Autore, M.; Cestelli Guidi, M.; Marcelli, A.; Schade, U.; Ito, Y.; Chen, M.; Lupi, S. Terahertz and mid-infrared plasmons in three-dimensional nanoporous graphene. *Nat. Commun.* **2017**, *8*, 14885.
7. Giorgianni, F.; Chiadroni, E.; Rovere, A.; Cestelli-Guidi, M.; Perucchi, A.; Bellaveglia, M.; Castellano, M.; Di Giovenale, D.; Di Pirro, G.; Ferrario, M.; Pompili, R.; Vaccarezza, C.; Villa, F.; Cianchi, A.; Mostacci, A.; Petrarca, M.; Brahlek, M.; Koirala, N.; Oh, S.; Lupi, S. Strong nonlinear terahertz response induced by Dirac surface states in Bi_2Se_3 topological insulator. *Nat. Commun.* **2016**, *7*, 11421.
8. Di Pietro, P.; Ortolani, M.; Limaj, O.; Di Gaspare, A.; Giliberti, V.; Giorgianni, F.; Brahlek, M.; Bansal, N.; Koirala, N.; Oh, S.; Calvani, P.; Lupi, S. Observation of Dirac plasmons in a topological insulator. *Nature Nanotech.* **2013**, *8*, 556–560.
9. Limaj, O.; Giorgianni, F.; Di Gaspare, A.; Giliberti, V.; de Marzi, G.; Roy, P.; Ortolani, M.; Xi, X.; Cunnane, D.; and Lupi, S.; Observation of Dirac plasmons in a topological insulator. *ACS Photonics* **2014**, *7*, 556–560.
10. Haxha, S.; AbdelMalek, F.; Ouerghi, F.; Charlton, M.D.B.; Aggoun, A.; Fang, X. Metamaterial Superlenses Operating at Visible Wavelength for Imaging Applications. *Sci. Rep.* **2018**, *8*, 16119.
11. Yang, J.J.; Huang, M.; Tang, H.; Zeng, J.; Dong, L. Metamaterial Sensors. *Int. J. Antennas Propag.* **2013**, *4*.
12. Macis, S.; Tomarchio, L.; Tofani, S.; Piccirilli, F.; Zacchigna, M.; Aglieri, V.; Toma, A.; Rimal, G.; Oh, S.; Lupi, S. Infrared plasmons in ultrahigh conductive $PdCoO_2$ metallic oxide. *Commun. Phys.* **2022**, *5*, 145.

13. Qin, M.; Pan, C.; Chen, Y.; Ma, Q.; Liu, S.; Wu, E; Wu, B. Electromagnetically Induced Transparency in All-Dielectric U-Shaped Silicon Metamaterials. *Appl. Sci.* **2018**, *8*, 10.

14. Oh, S.S.; Hess, O. Chiral metamaterials: enhancement and control of optical activity and circular dichroism. *Nano Converg.* **2015**, *2*, 24.

15. Gil, M.; Bonache, J.; Martín, F. Metamaterial filters: a review. *Int. J. Antennas Propag.* **2008**, *4*, 186–197.

16. Dong, Y.; Yu, D.; Li, G.; Lin, M.; Bian, L-A. Terahertz Metamaterial Modulator Based on Phase Change Material VO_2 . *Symmetry* **2021**, *13*, 2230.

17. Anlage, S. M. The physics and applications of superconducting metamaterials. *J. Opt.* **2011**, *13*, 024001.

18. Jung, P.; Ustinov, A. V.; Anlage, S. M. Progress in superconducting metamaterials. *Supercond. Sci. Technol.* **2014**, *27*, 073001.

19. Lobo, R.P.S.M.; Bontemps, N.; Racah, D.; Deutscher, G. Pseudo-gap and superconducting condensate energies in the infrared spectra of Pr-doped $YBa_2Cu_3O_7$. *EPL* **2001**, *55*, 854–860.

20. Garcia-Garcia, J.; Martin, F.; Baena, J. D.; Marques, R.; Jelinek, L. On the resonances and polarizabilities of split ring resonators. *J. Appl. Phys.* **2005**, *98*, 033103.

21. Bitzer, A.; Merbold, H.; Thoman, A.; Feurer, T.; Helm, H.; Walther, M. Terahertz Near-Field Imaging of Electric and Magnetic Resonances of a Planar Metamaterial. *Opt. Express* **2009**, *17*, 5, 3826–34.

22. Bitzer, A.; Ortner, A.; Merbold, H.; Feurer, T.; Walther, M. Terahertz Near-Field Microscopy of Complementary Planar Metamaterials: Babinet's Principle. *Opt. Express* **2011**, *19*, 2537–2545.

23. Falcone, F.; Lopetegi, T.; Laso, M.; Baena, J. D.; Bonache, J.; Beruete, M.; Marqués, R.; Martín, F.; Sorolla, M. Babinet Principle Applied to the Design of Metasurfaces and Metamaterials, *Phys. Rev. Lett.* **2004**, *93*.

24. Klein, M. W.; Enkrich, C.; Wegener, M.; Soukoulis, C. M.; Linden, S.; Single-slit split-ring resonators at optical frequencies: limits of size scaling. *Opt. Lett.* **2006**, *31*, 1259–61.

25. Jin, B.; Zhang, C.; Engelbrecht, S.; Pimenov, A.; Wu, J.; Xu, Q.; Cao, C.; Chen, J.; Xu, W.; Kang, L.; Wu, P. Low Loss and Magnetic Field-tuned Superconducting THz Metamaterial. *Opt. Soc. Am.* **2010**.

26. Garcia-Garcia, J.; Bonache, J.; Gil, I.; Martin, F.; Velazquez-Ahumada, M.C.; Martel, J. Miniaturized microstrip and CPW filters using coupled metamaterial resonators. *IEEE Trans. Microw. Theory. Tech.* **2006**, *54*, 6, 2628–2635.

27. Chen, H.-T.; Yang, H.; Singh, R.; O'Hara, J.F.; Azad, A.K.; Trugman, S.A.; Jia, Q.X.; Taylor, A.J. Tuning the Resonance in High-Temperature Superconducting Terahertz Metamaterials. *Phys. Rev. Lett.* **2010**, *105*, 247402.

28. Kiwa, T.; Tonouchi, M. High frequency properties of YBCO thin films diagnosed by time-domain terahertz spectroscopy. *Physica C* **2001**, *362*, 314–318.

29. Klein, N. High-frequency applications of high-temperature superconductor thin films. *Rep. Prog. Phys.* **2002**, *65*, 1387–1425.

30. Gao, F.; Whitaker, J.F.; Uher, C. High-Frequency Surface Impedance and Penetration Depth of $YBa_2Cu_3O_7$ Films: Coherent Time-Domain Spectroscopy Method. *IEEE Trans. Appl. Supercond.* **1995**, *5*, 2.

31. Dressel, M.; Grüner, G. *Electrodynamics of Solids* Cambridge University Press, 2002, pp. 28–30, 42–44, 372–377.

32. Limaj, O.; Giorgianni, F.; Di Gaspare, A.; Giliberti, V.; de Marzi, G.; Roy, P.; Ortolani, M.; Xi, X.; Cunnane, D.; Lupi, S. Superconductivity-Induced Transparency in Terahertz Metamaterials. *ACS Photonics* **2014**, *1*, 7, 570–575.

33. Wallace, G.Q.; Lagugné-Labarthet, F. Advancements in fractal plasmonics: structures, optical properties, and applications. *Analyst* **2019**, *144*, 7, 13–30.

34. Panaro, S.; Nazir, A.; Proietti Zaccaria, R.; Razzari, L.; Liberale, C.; De Angelis, F.; Toma, A. Plasmonic Moon: A Fano-Like Approach for Squeezing the Magnetic Field in the Infrared. *Nano Lett.* **2015**, *15*, 6128–6134.